Supporting Information

Deciphering the Cooperative Roles of NH_4^+ and H^+ in Aqueous Ammonium-Ion Batteries

Sungjin Yang[1], Min Soo Jung[1], Maxine A. McNerney[1], Jungwook Song[1,2], Yanzhao Fang[1], Xiulei Ji[1]*

[a] Department of Chemistry, Oregon State University, Corvallis, Oregon 97331, United States

Email: david.ji@oregonstate.edu

[b] Department of Chemistry, Dong-A University, Busan, 49315, South Korea

Materials Preparation

Copper hexacyanoferrate (CuHCF) was synthesized through a conventional co-precipitation method. A 200 mL aqueous solution of $CuSO_4$ (0.16 M) was slowly added dropwise into 200 mL of a $K_3[Fe(CN)_6]$ solution (0.10 M) under continuous stirring. The resulting suspension was stirred overnight to ensure complete precipitation, followed by sequential washing with deionized water (three times) and ethanol (once).[1] As is typical for Prussian blue analogue frameworks synthesized in aqueous media, the resulting CuHCF is expected to contain $[Fe(CN)_6]$ vacancies accompanied by structural (coordination and/or zeolitic) water; thus, it exists as a hydrated, non-stoichiometric framework, in which the actual Cu:Fe ratio may deviate from the precursor feed ratio.

For electrochemical measurements, CuHCF working electrodes were prepared by mixing 70 wt% CuHCF, 20 wt% Ketjenblack (KB), and 10 wt% poly(vinylidene fluoride) (PVdF) in 1-methyl-2-pyrrolidone (NMP) to form a uniform slurry. The slurry was uniformly cast onto carbon paper substrates (AvCarb P75) and subsequently dried at 80 °C to remove residual solvent.

For *ex situ* X-ray diffraction (XRD) characterization, free-standing CuHCF films were fabricated by blending 70 wt% CuHCF, 20 wt% KB, and 10 wt% polytetrafluoroethylene (PTFE) binder in 2-propanol until a homogeneous paste was obtained, followed by rolling and drying under ambient conditions. For electrochemical impedance spectroscopy (EIS), free-standing electrodes were prepared using a similar procedure but with an optimized composition of 80 wt% CuHCF, 10 wt% KB, and 10 wt% PTFE to ensure high mechanical integrity and sufficient electronic conductivity. Activated carbon (AC) free-standing-film counter electrodes were prepared in the same manner as above using 70 wt% activated carbon, 20 wt% KB, and 10 wt% PTFE as the active, conductive, and binding components, respectively.

Materials Characterization

X-ray diffraction (XRD) measurements were carried out on a Rigaku MiniFlex diffractometer equipped with a Cu Kα radiation source (λ = 1.5406 Å) operated at 40 kV and 15 mA. Diffraction patterns were collected over a 2θ range of 10^o-80^o at a scan rate of 2° min^{-1}. The obtained data were used to identify the crystalline phase and evaluate structural changes of the CuHCF electrodes after electrochemical cycling.

Electrochemical Characterization

Galvanostatic cycling tests were performed using three-electrode Swagelok cells, with CuHCF coated on carbon paper as the working electrode (WE), a free-standing film of AC as the counter electrode (CE), and AgCl/Ag (3 M KCl) as the reference electrode (RE). Glass fiber filter papers (GF/A grade, Whatman, Inc.) were used as separators. The cells were tested by a battery cycler

(CT3002A, Landt Instruments, Inc.) for performance testing, operated at a constant current rate of 0.2 A g^{-1}.

For isotope-substitution experiments, identical cell configurations were used, except that the aqueous electrolyte was prepared with D_2O as the solvent instead of H_2O. All electrodes and reference electrodes (AgCl/Ag, 3 M KCl) were used without modification.

Cyclic voltammetry (CV), Tafel, and EIS measurements were performed using a VMP-3 multichannel potentiostat (Bio-Logic).

A flat-membrane pH electrode (BlueLine 27 pH, WTW-XYLEM; SenTix® Sur) was connected to the side of working electrode to record local interfacial potential variations, which were used as a proxy for relative changes in interfacial proton activity in real time. For *operando* pH measurements during galvanostatic cycling, two channels of the VMP-3 potentiostat were configured in the CE-to-ground mode to avoid electrical interference. The CE was grounded and shared between the two channels, with the primary channel performing galvanostatic cycling and the secondary channel simultaneously recording the open-circuit voltage (OCV) using the pH electrode. The measured potentials were converted to relative pH values according to the calibration equation E (mV) = –57 (mV) · pH + 395 (mV), which was obtained through direct experimental calibration using standard buffer solutions.

The pH microelectrode was positioned in close proximity to, and in controlled contact with, the electrode surface to probe local interfacial pH variations, with contact ensured by the Swagelok cell assembly. A narrow Ti foil current collector was present between the electrode and the probe, which may introduce partial shadowing and local concentration gradients near the probe.

While such geometric and diffusion-related effects cannot be entirely excluded, they are expected to introduce largely static or slowly varying offsets in the measured pH rather than the time-dependent pH transients discussed in this work. Accordingly, the *operando* pH measurements are interpreted in a qualitative and comparative manner, focusing on relative and transient changes in local proton activity rather than absolute interfacial pH values. Within this framework, the observed pH evolution is interpreted as reflecting dynamic interfacial processes that modulate electrochemical states, rather than direct bulk charge-storage reactions.

CV tests were conducted in asymmetric three-electrode Swagelok cells, employing CuHCF coated on carbon paper as the WE, AC as the CE, and AgCl/Ag (3 M KCl) as the RE.

Tafel analyses were carried out in three-electrode configurations, with CuHCF on carbon paper as the WE, graphite rods as the CE, and AgCl/Ag (3 M KCl) as the RE. Polarization curves were recorded at a scan rate of 10 mV min^{-1}.

Galvanostatic EIS (GEIS) for distribution of relaxation times (DRT) analyses was performed using asymmetric three-electrode Swagelok cells, with CuHCF on carbon paper as the WE, AC as the CE, and AgCl/Ag (3 M KCl) as the RE, during galvanostatic cycling at 0.05 A g^{-1}. A sinusoidal current amplitude of 10 mA was applied over a frequency range from 200 kHz to 1 Hz. Each GEIS spectrum was collected with an acquisition time of 44 s, and data points in the low-frequency region were excluded due to excessive noise. The DRT spectra, expressed as γ(ln τ) versus τ, were obtained using the MATLAB implementation of the method developed by Wan et al. with default fitting parameters.[2]

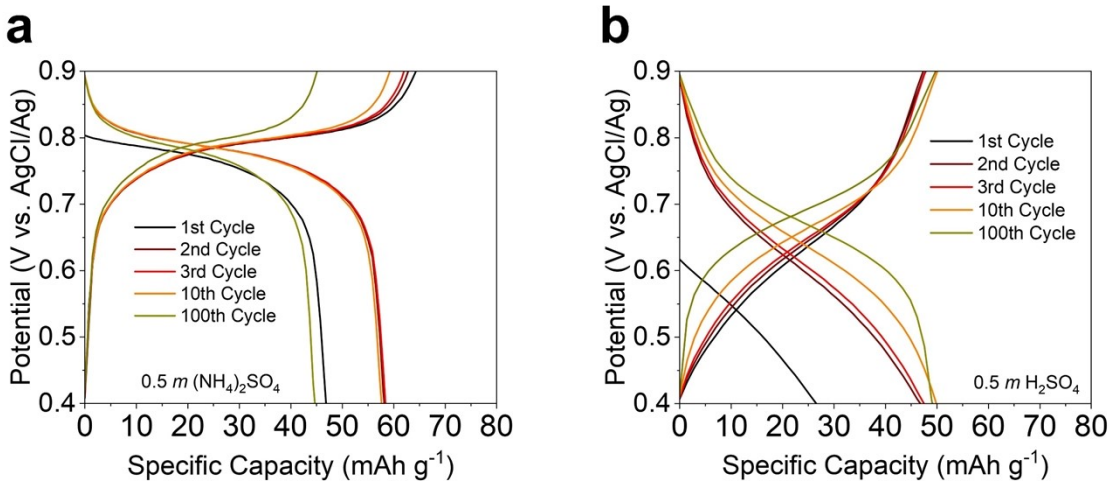

Figure S1. Galvanostatic charge–discharge (GCD) profiles of CuHCF electrodes in (a) 0.5 *m* $(NH_4)_2SO_4$ and (b) 0.5 *m* H_2SO_4 electrolytes, collected at 0.5 A g^{-1}.

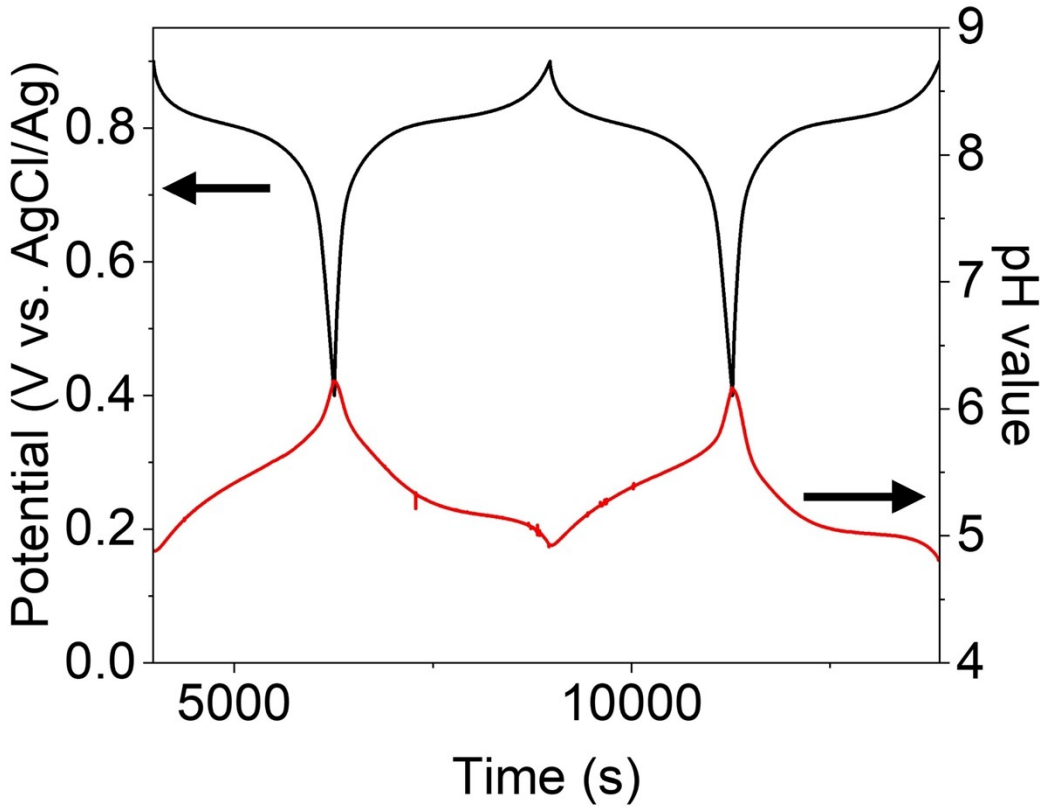

Figure S2. *Operando* potential (black) and pH (red) profiles of the CuHCF electrode during the second galvanostatic cycle in the 0.5 *m* $(NH_4)_2SO_4$ electrolyte prepared with D_2O.

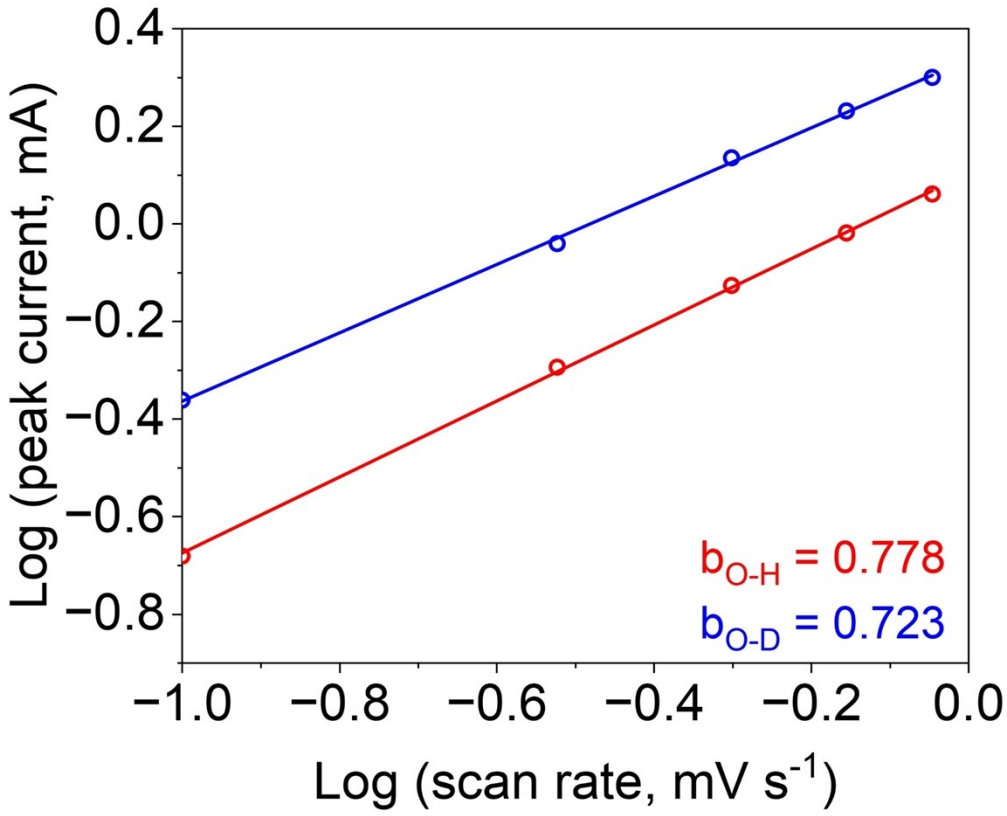

Figure S3. Log(i) – log(v) plots derived from anodic peak currents of CuHCF electrodes measured in 0.5 *m* $(NH_4)_2SO_4$ electrolytes prepared with H_2O and D_2O.

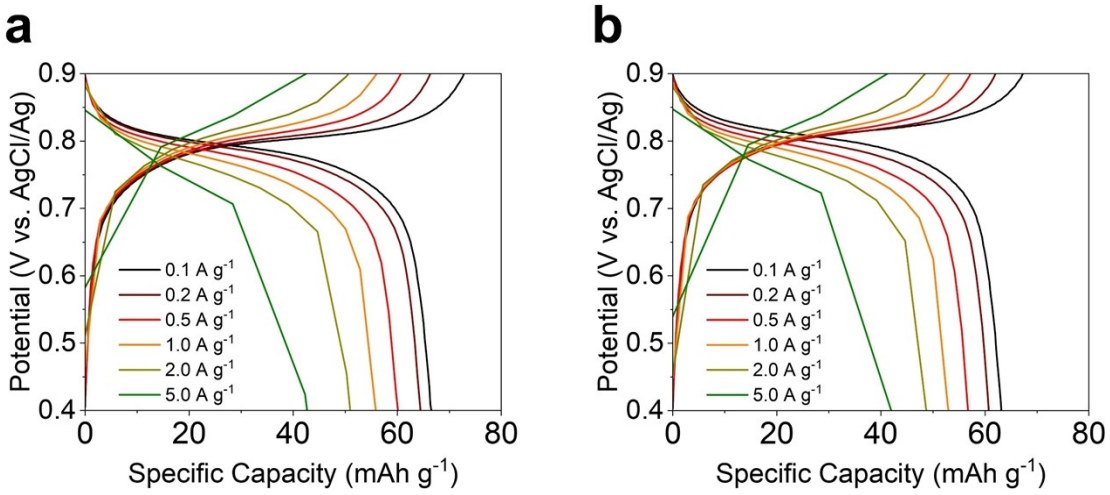

Figure S4. GCD profiles of CuHCF electrodes in (a) H_2O-based and (b) D_2O-based 0.5 *m* $(NH_4)_2SO_4$ electrolytes at various current rates (0.1-5.0 A g^{-1}). Each curve represents the middle cycle among five repeated cycles at the corresponding current rates.

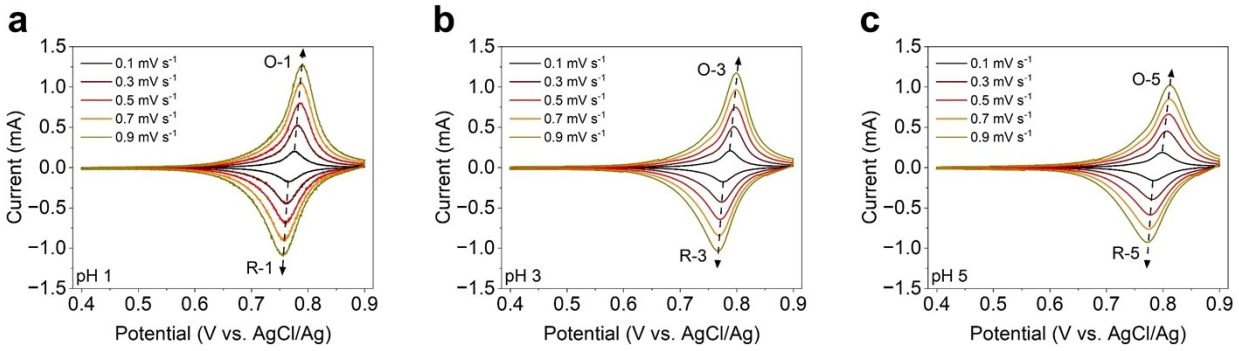

Figure S5. CV curves of CuHCF electrodes recorded at various scan rates in 0.5 *m* $(NH_4)_2SO_4$ electrolytes adjusted to (a) pH 1, (b) pH 3, and (c) pH 5.

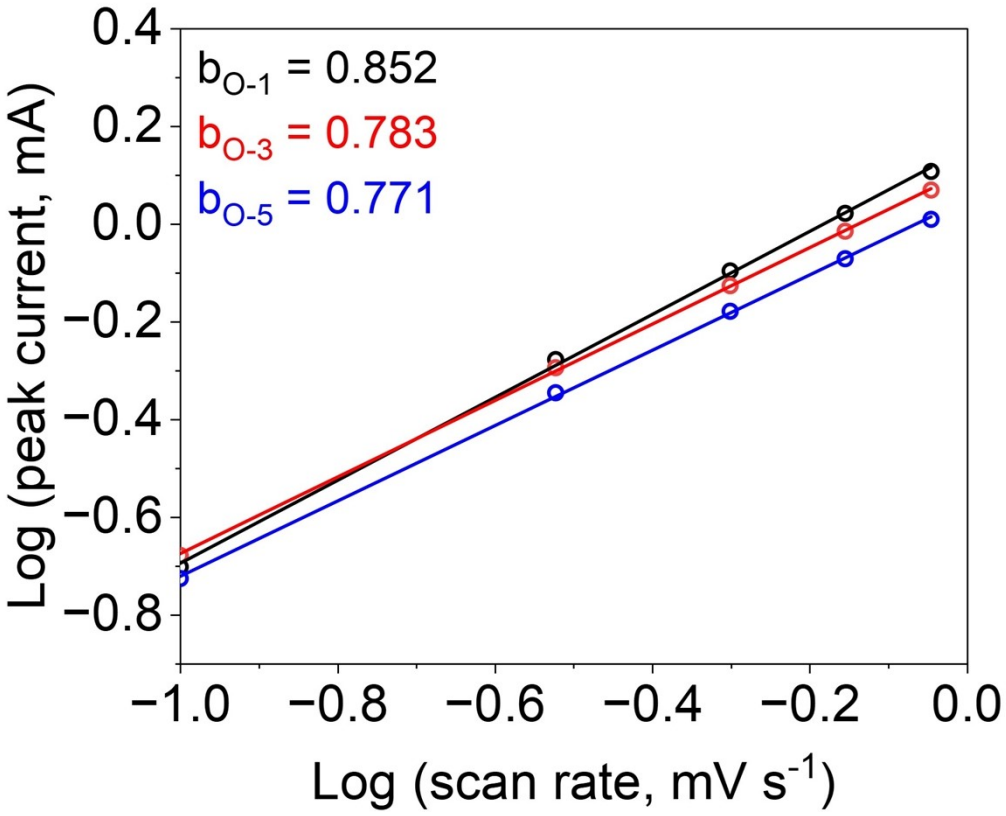

Figure S6. Log(i)–log(v) plots derived from anodic peak currents of CuHCF electrodes measured in 0.5 *m* $(NH_4)_2SO_4$ electrolytes at pH 1, 3, and 5.

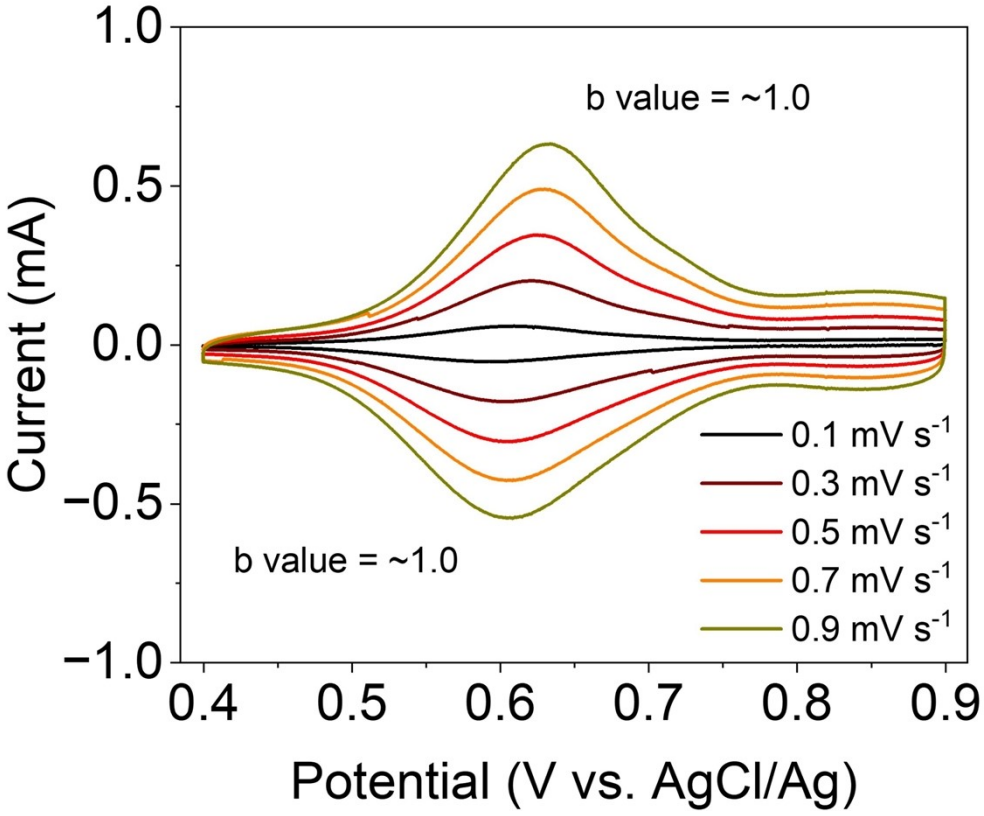

Figure S7. CV curves of CuHCF electrodes in 0.5 *m* H_2SO_4 electrolyte at various scan rates.

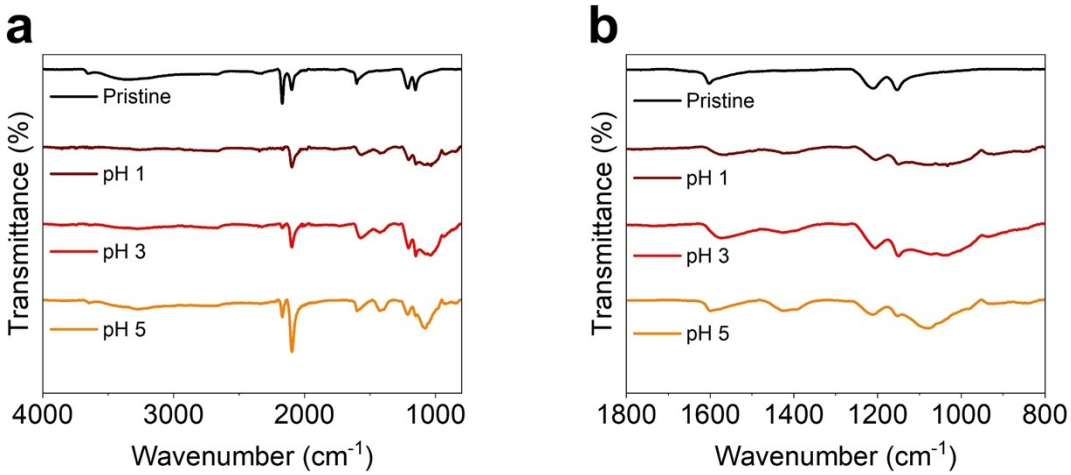

Figure S8. Ex situ FTIR spectra of CuHCF electrodes collected after 100 charge–discharge cycles at 0.1 A g^{-1} in 0.5 *m* $(NH_4)_2SO_4$ electrolytes with different pH values (1, 3, and 5), along with the pristine electrode before cycling: **(a)** full wavenumber range (4000–800 cm^{-1}) and **(b)** enlarged fingerprint region (1800–800 cm^{-1}).

The observed spectral variations after cycling are limited to intensity changes and minor features, without discernible shifts in peak positions or the emergence of new vibrational modes. Accordingly, no specific chemical decomposition or bulk framework collapse is inferred from these spectra, which are intended to serve as qualitative boundary-setting evidence.

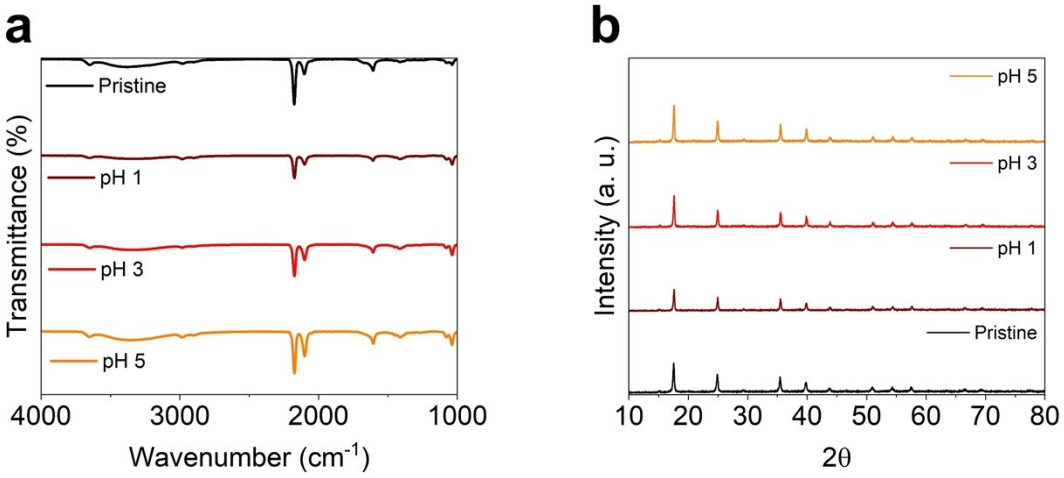

Figure S9. Ex situ (a) FTIR spectra and (b) XRD patterns of pristine CuHCF powder and samples after soaking in 0.5 *m* $(NH_4)_2SO_4$ electrolytes adjusted to pH 1, 3, and 5 for 72 h, in the absence of electrochemical cycling.

Variations in peak intensity are not taken as evidence of chemical decomposition or framework collapse.

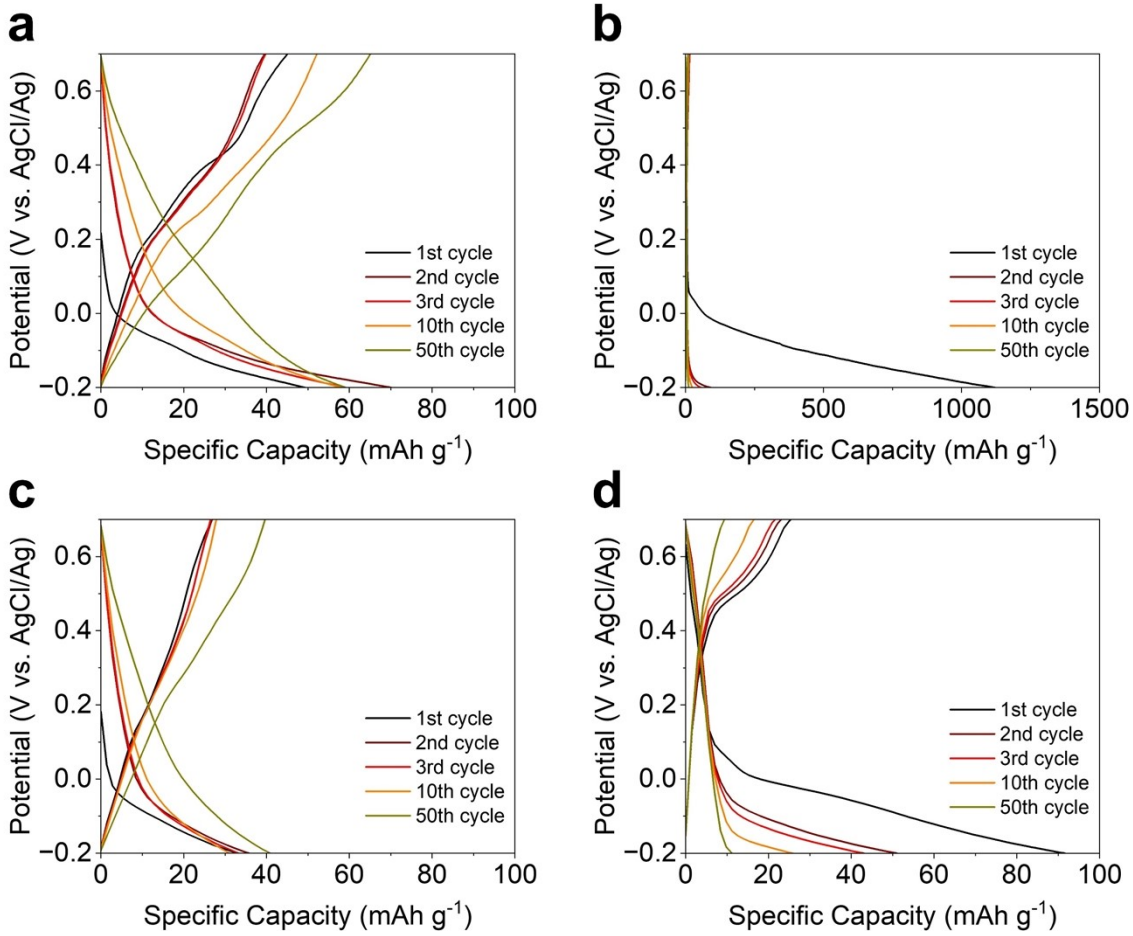

Figure S10. GCD profiles of V_2O_5 electrodes cycled in (a) 0.5 *m* $(NH_4)_2SO_4$ and (b) 0.5 *m* H_2SO_4 at 0.2 A g^{-1}, and (c) 0.5 *m* $(NH_4)_2SO_4$ and (d) 0.5 *m* H_2SO_4 at 0.5 A g^{-1}.

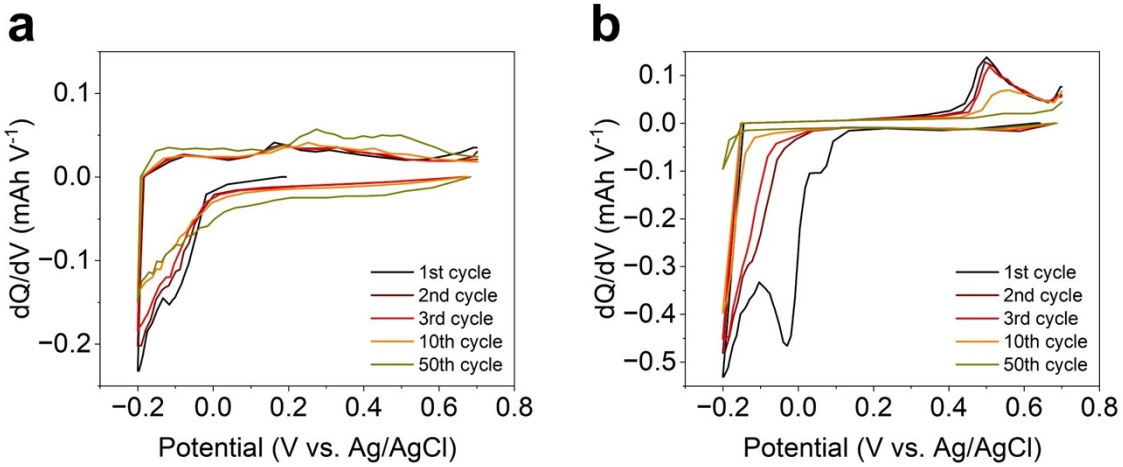

Figure S11. Differential capacity (dQ/dV) profiles derived from the GCD data shown in **Figure S9** for V_2O_5 electrodes in (a) 0.5 *m* $(NH_4)_2SO_4$ and (b) 0.5 *m* H_2SO_4 electrolytes, collected at 0.5 A g^{-1} for selected cycles.

Figures S10 and **S11** present galvanostatic cycling and corresponding differential-capacity (dQ/dV) profiles of V_2O_5 electrodes in ammonium-salt and proton-rich electrolytes. While plateau-like features are observed in both cases, the cycling stability and dQ/dV lineshapes exhibit clear electrolyte-dependent differences, indicating that proton-rich environments can significantly influence electrochemical signatures in a host-dependent manner. No mechanistic assignment is attempted for V_2O_5, as these data are intended solely as a qualitative comparison.

References

1 X. Wu, J. J. Hong, W. Shin, L. Ma, T. Liu, X. Bi, Y. Yuan, Y. Qi, T. W. Surta, W. Huang, J. Neuefeind, T. Wu, P. A. Greaney, J. Lu and X. Ji, *Nat. Energy*, 2019, 4, 123–130.

2 T. H. Wan, M. Saccoccio, C. Chen and F. Ciucci, *Electrochim. Acta*, 2015, 184, 483–499.